Wind and soil model influences on the uncertainty in fatigue of monopile supported wind turbines

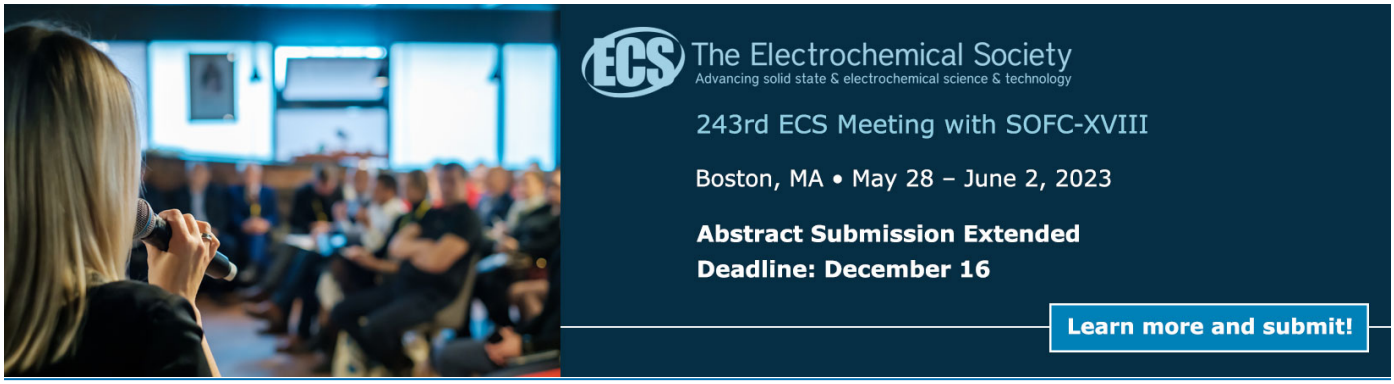

Wind and soil model influences on the uncertainty in fatigue of monopile supported wind turbines

SH Sørum, EE Bachynski-Polić and J Amdahl

Centre for Autonomous Marine Operations and Systems, Department of Marine Technology, NTNU, 7491 Trondheim, Norway

E-mail: stian.h.sorum@ntnu.no

Abstract. Several alternative engineering models are available for the use in analysis of offshore wind turbines. However, it is not always clear which of the models will yield the most accurate or sufficiently conservative results. This paper investigates the effect of using two alternative soil-structure interaction models and two wind coherence models. The focus is on assessing how these modelling choices influence the predicted long-term fatigue damage in the support structure. The two soil models are a macro-element model and a p-y-curve model with Rayleigh damping. This gives differences in both the damping and stiffness properties of the turbine model. The differences between the two soil models tend to decrease as the turbine size increases. The wind coherence models considered are the Kaimal spectrum with exponential coherence and the Mann uniform shear turbulence model. The Kaimal model predicts the highest response at low frequencies, while the Mann model gives the highest response predictions at higher frequencies. Which turbulence model predicts the highest long-term fatigue damage is then determined by the natural frequencies, rotor and blade passing frequencies of the different turbines.

1. Introduction

Several engineering models may be selected for analysis of offshore wind turbines (OWTs). Different models may yield different results and thereby give different designs. Further, it is often unclear which of the available models are most accurate. They may be based on different assumptions, incorporate different physical effects, or be developed for different applications.

This paper will investigate the influence of using different models for two aspects of the fatigue analysis of monopile supported OWTs. Both the soil-structure interaction (SSI) and wind coherence models influence the response prediction, and thereby the design fatigue lifetime, of OWTs. While previous studies have looked into both the model development and short-term response, this paper will focus on the long-term effects of using the different models. As the difference between the models vary with turbine size, three turbines in the size range 5 to 15 MW are considered. Finally, the influence of uncertainty in the site parameters (e.g. turbulence intensity and soil stiffness) is investigated.

1.1. Soil Modelling

Traditionally, SSI was modelled with p-y curves, based on experience from the offshore oil and gas industry[1]. These represent the soil resistance as non-linear elastic springs distributed along the length of the pile. While still used, the PISA project showed the need for modifying

the curves for the offshore wind industry[2]. Other methods have been developed, such as the apparent fixity method, and the use of linear stiffness and damping matrices[3, 4, 5]. Aasen et al.[5] also used a 1D rotational element fixed below seafloor, with many properties similar to the macro element developed by Page et al.[6, 7] The study showed a difference of up to 4 years in predicted lifetime when using the different soil models[5]. Katsikogiannis et al.[8] found differences of up to 180% in the short-term fatigue damage between the macro-element and p-y-curve approach in cases with negligible aerodynamic damping. In this paper, the difference between the macro-element model and p-y-curve approach will be further investigated.

1.2. Wind Coherence Modelling

The IEC standard[9] recommends two models for the wind field when analysing OWTs: The Kaimal spectral model with exponential coherence (denoted "Kaimal model" hereafter) and the Mann uniform shear turbulence model (hereafter denoted the "Mann model"). It is expected that the two models show larger deviations as turbine size increases. Several studies have investigated the difference between these two models. Myrtvedt, Nybø & Nielsen[10] and Nybø, Nielsen & Godvik[11] both investigated the response of a bottom-fixed 10-MW turbine, showing the largest difference at stable conditions[11] and at close to rated wind speeds[10]. Bachynski & Eliassen[12] investigated the response of a 5-MW turbine on several floating support structures, and found differences of up to 40% in the standard deviation of the floater motions. Wise & Bachynski[13] showed that the Kaimal model yields a higher response at low frequencies and a lower response at high frequencies, also this for floating turbines. The same was observed at 3P frequencies by Bachynski & Eliassen[12].

2. Model Description

This study considers three turbine models; the NREL 5-MW[14], DTU 10-MW[15] and IEA 15-MW[16] reference wind turbines. The turbines are assumed located on the Norwegian Continental Shelf, at a water depth of 30 m. The soil conditions at the site are assumed to be an idealized clay profile with quadratic variation of the shear modulus with depth and linearly increasing undrained shear strength. The 5-MW monopile is from the OC3 project[17], while the 10-MW foundation is based on Velarde and Bachynski[18]. The 15-MW tower is the IEA design, and the monopile is designed for a natural period below 5.5 s. The fatigue capacity of the latter was checked using equivalent sea states[19]. Table 1 summarizes the properties of the turbines.

Table 1. Key parameters of the turbines in the study.

Parameter	Unit	NREL	DTU	IEA
Rated power	MW	5	10	15
Rated wind speed	m/s	11.4	11.4	10.59
Rated rotor speed	rpm	12.1	9.6	7.56
Rotor diameter	m	126	178.3	240
Hub height	m	90	119	150
Monopile diameter	m	7	9	11
Monopile wall thickness	m	0.07	0.11	0.11
1st fore-aft natural period	s	3.9	3.6	5.3

2.1. Environmental Model

The environmental model assumes the distribution of the wave parameters are conditional on the wind speed, with the wind direction as an independent variable. For each wind speed, a single sea state is used to represent the sea state distribution[19]. This gives the probability of occurrence for an environmental condition as

$$P(U_i, \theta_{wi,j}, \theta_{rel,k}) = P_n(U_i) \cdot P(\theta_{wi,j}) \cdot P_n(\theta_{rel,k}|U_i). \quad (1)$$

$P_n(U_i)$ is the probability of occurrence for wind speed U_i, $P(\theta_{wi,j})$ is the probability of occurrence of wind direction $\theta_{wi,j}$ and $P_n(\theta_{rel,k}|U_k)$ is the probability of occurrence for wind-wave misalignment bin $\theta_{rel,k}$. Three wind speed bins are considered: close to rated (8-10 m/s), intermediate (14-16 m/s) and high (20-22 m/s), while two misalignment angles (0°and 30°) are included. The distribution of the environmental parameters are based on 60 years of data from the NORA10 hindcast data base[20]. $P_n(U_i)$ and $P_n(\theta_{rel,k}|U_k)$ are normalized to give a total probability of 1 for the environmental conditions considered. Further details are given by Sørum et al.[21] The wave elevation is modelled using a Pierson-Moskowitz spectrum for the lowest wind speed and a JONSWAP spectrum for the two higher wind speeds.

2.2. Load Models

Hydrodynamic loads are calculated using linear wave kinematics, and MacCamy & Fuchs load model[22] combined with Morison-type drag loads. The hydrodynamic added mass is assumed to correspond to an added mass coefficient of 1.0.

Aerodynamic loads on the blades are calculated using unsteady blade element momentum theory with Glauert induction and Prandtl tip loss corrections for the operational turbine. Dynamic stall and dynamic wake correction is also included. For the parked turbine, aerodynamic loads are calculated based on the undisturbed wind field. The Kaimal turbulence model with exponential coherence and the Mann turbulence model are both used in this study, although only the Kaimal model is utilized when investigating the effect of the different soil models. Wind shear is modelled using the power law formulation.

2.3. Simulation Models

The wind turbine, tower and monopile above seafloor are modelled in SIMO-Riflex, an aero-hydro-servo-elastic simulation tool from SINTEF Ocean[23, 24]. Linear-elastic beam elements are used to model the structural components above seafloor.

2.4. Foundation Models

The two foundation models used in this study are a macro-element formulation and a p-y-curve model. In the part of the study investigating the effect of wind coherence models, only the macro element has been used.

A macro element reduces the soil-structure interaction to a load-displacement relationship at the seafloor, which reduces the simulation time. The macro element used here accounts for the non-linear load-displacement relationship of monopile OWTs at the seafloor and takes into account the different loading and offloading characteristics of the soil. This introduces hysteretic damping into the model. A more detailed description of the model is given by Page et al.[7]. The macro element is connected to the structural model at seafloor. A post-processing tool based on beam elements with springs is applied for determining the monopile loads below this[25].

The p-y curves are modelled as non-linear elastic springs attached to the beam model of the monopile below seafloor. Soil damping is accounted for by increasing the structural damping, which is tuned to give the same average damping coefficient as the macro element in a decay test starting from rated thrust.

Both the macro element, the post-processing tool and the p-y curves are calibrated to the soil-structure interaction found by a 3D continuum finite element analysis performed in Plaxis.

2.5. Fatigue Damage Calculation

Fatigue damage is calculated based on the axial stress variations in the tower and monopile. The individual stress cycles are extracted using the rainflow counting technique in WAFO[26], modified to allow for bi-linear SN curves. Miner's sum with thickness correction[27] is used to calculate the fatigue damage. The fatigue utilization is found as the ratio between the calculated fatigue damage and the fatigue capacity, Δ_C. DNV's SN-curve "D" for steel in sea water is used for the monopile, while the curve for steel in air is used for the tower.

2.6. Parameter Variations

To investigate if there is a coupling between the model variations and site parameters, the turbines were analysed using random realizations of 16 parameters. These parameters represent the uncertainty in a fixed design, and include uncertainty in the environmental description, soil uncertainty, fatigue parameter uncertainties and more. A list of the parameters is given in Appendix A, with the data source or reference for the distributions. 30 samples were used, with details on distributions and sampling strategy given by Sørum et al.[21]. Results from the individual realizations are used only when investigating the coupling (Sections 4.4 and 5.5) and when extracting response spectra. The remaining results are mean values across all realizations.

3. Fatigue Damage Utilization

The maximum long-term fatigue damage utilization along the support structure is shown in Figure 1, with $z = 0$ representing the sea floor. The lines represent the mean value of the 30 samples of the design parameters described in Section 2.6. Three locations of interest are identified in the support structures. The fatigue damage in the tower top is mainly caused by the rotor pitching moment. In the tower base, the loads are primarily caused by the aerodynamic thrust force and the wave-induced inertia loads. Finally, the loading at seafloor is caused by both aerodynamic loads and wave loads. The latter is also representative for the location with the highest fatigue utilization in the monopile, approximately one pile diameter below seafloor.

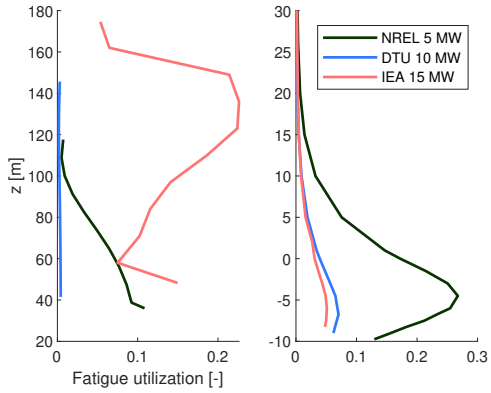

Figure 1. Maximum lifetime fatigue utilization in the tower (left) and monopile (right). Note that the transition pieces and lower parts of the monopiles are excluded.

4. Effects of Soil Model

The following sections will demonstrate how the differences between the two soil models influence the basic properties of the turbine models, followed by an assessment of the effect on the long-term fatigue damage.

4.1. Effect on Natural Frequency and Damping

The differences between the SSI models introduce differences in both the natural frequency and damping properties of the models. This is illustrated by decay tests, measuring the natural frequency and damping ratio in percent of critical damping for the different turbines.

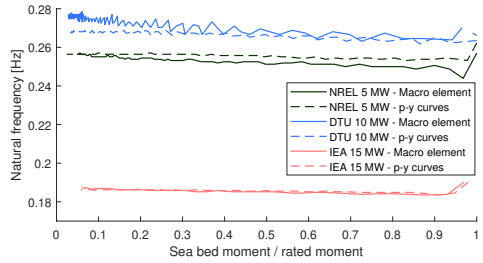

Figure 2. Natural frequencies, with no thrust force.

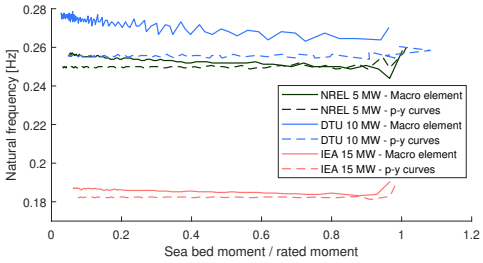

Figure 3. Natural frequencies, at rated thrust.

Figure 2 shows the fore-aft natural frequencies as function of the measured bending moment at the seafloor with zero mean load. The p-y model shows little variation in natural frequency with amplitude, while the macro-element model has a clear trend of the natural frequency decreasing with increasing response amplitude. The amplitude-dependency of the natural frequency is largest for the 5-MW turbine and smallest for the 15-MW turbine. Including the rated thrust as a mean load, the natural frequency is reduced when using the p-y curves as shown in Figure 3. The change is most significant for the smallest turbine. Depending on the mean load and response amplitude, the two soil models may then yield both lower and higher natural frequencies than the other.

Figure 4. Damping ratio NREL 5-MW turbine.

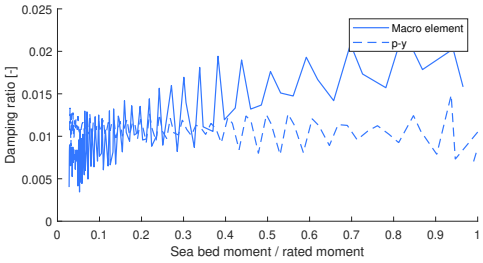

Figure 5. Damping ratio DTU 10-MW turbine.

The soil models also show a difference in how damping is included. The amplitude-dependent damping of the macro element is shown in Figures 4 to 6. This shows how the damping in the macro-element models increase with amplitude. The opposite is seen for the p-y curves, where the damping is amplitude-independent. Due to the tuning of the damping for the latter model, the amplitude for which the two SSI models predict the same damping also varies.

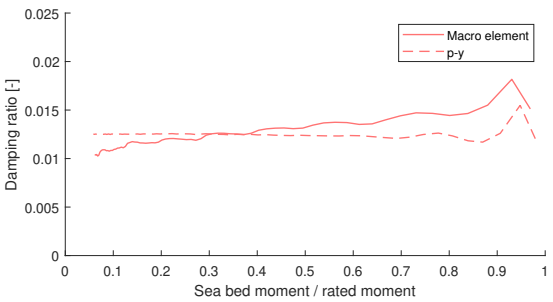

Figure 6. Damping ratio IEA 15-MW turbine.

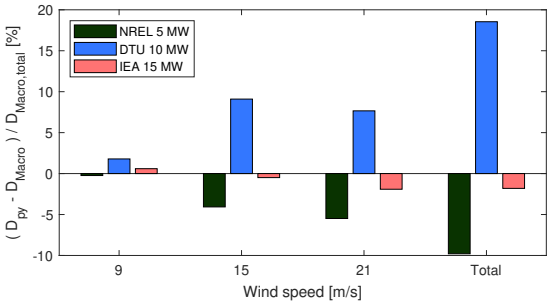

Figure 7. Difference in fatigue damage predictions at seafloor using the macro-element and p-y-curve models.

4.2. Response Above Seafloor

The effect of changing the soil model is similar across the support structure above seafloor, but with diminishing differences close to the tower top. However, as shown in Figure 7 there is a significant difference between the turbines. This figure shows the difference in the lifetime fatigue damage predicted per wind speed, and is normalized by the total fatigue damage predicted using the macro-element model. For both the 5-MW and 15-MW turbines, the macro element yields the highest fatigue damage. The opposite is the case for the 10-MW turbine, which also shows the highest difference between the models.

The 5-MW turbine shows a lower fatigue damage estimate when using the p-y curves for all wind speeds. Figures 8 and 9 illustrate the reason: Both the stiffness and damping are higher when using the p-y curves, leading to a reduced response and a lower fatigue damage. This trend is not universally true, amongst other it depends on the whether the response is in line with the wind or in the cross-wind direction. Still, the majority of the load cases show this trend, resulting in a higher fatigue damage prediction when using the macro-element model.

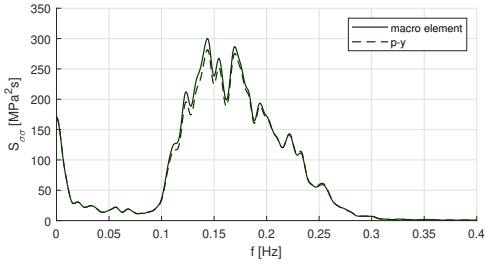

Figure 8. Upwind stress spectra at seafloor for the 5-MW turbine when operating at wind speed 15 m/s.

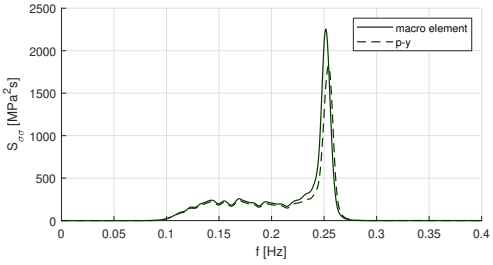

Figure 9. Upwind stress spectra at seafloor for the 5-MW turbine when parked at wind speed 15 m/s.

For the 10-MW turbine the opposite is the case: In a majority of the load cases the highest stiffness and damping is seen for the macro element, and a higher prediction of fatigue damage above seafloor is seen when using the p-y-curve model. Finally, the difference between the two models is smaller for the 15-MW turbine. This is also seen in Figures 2, 3 and 6, where there is a close match between the natural frequency and damping of the two soil models.

4.3. Response Below Seafloor

A different picture is seen below seafloor, illustrated in Figure 10 for the location in the monopile with highest fatigue damage. The first trend is that the difference between the models is more positive/less negative than above seafloor, indicating that the p-y model predicts higher responses when moving down into the soil. The reason is illustrated in Figure 11 for the 15-MW turbine. In the stiffness-dominated low frequencies, there is a good agreement between the macro-element (solid line) and p-y-curve (dashed line) response both at the sea floor (pink lines) and at the location with highest fatigue damage (black lines). However, there is a difference around the natural frequency (∼0.18 Hz). Here, the damping provided by the macro element is higher when moving down into the soil. This leads to larger response amplitudes, and increased fatigue damage predictions below sea floor when using the p-y-curve model.

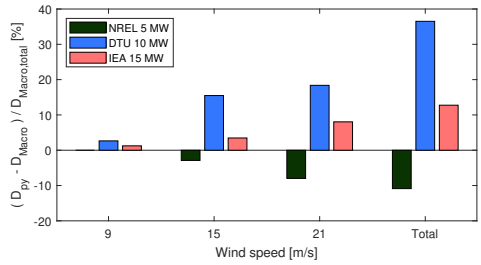

Figure 10. Difference in fatigue damage predictions below seafloor using the macro-element and p-y-curve models.

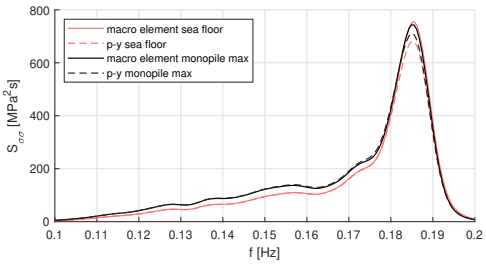

Figure 11. Upwind stress spectra at seafloor and below seafloor for the parked 15-MW turbine.

4.4. Interaction with Uncertain Design Parameters

Figure 12 shows the difference in fatigue prediction when using the two soil models versus the undrained shear strength. The latter is varied as described in Section 2.6. Increased shear strength reduces the fatigue damage predictions of the p-y-curve model, compared to the macro element. No other interactions were seen between the design parameters and the soil model.

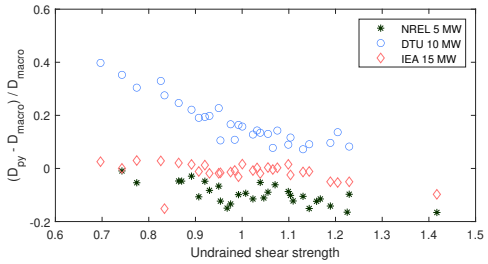

Figure 12. Difference in fatigue prediction for the soil models versus undrained shear strength.

5. Effects of Wind Model

This section presents the effect of varying the wind coherence models, starting with a description of the coherence properties before the turbine response is analysed.

5.1. Differences Between Wind Fields

When looking at the characteristics of the wind field simulated by the Kaimal and Mann models, two properties are of primary interest. The first is the spectral coherence, describing the relationship between the the wind speed at two different spatial locations. In the Kaimal model, this is described by an exponential coherence function, while the Mann model uses a velocity tensor model. To evaluate influence on coherence, the coherence of the wind speed at the hub and at the outer edge of the rotor disk at hub height is calculated. This is defined as

$$\gamma_{xy}(f) = \frac{S_{xy}(f)}{\sqrt{S_{xx}(f)S_{yy}(f)}} = C_{xy}(f) + iQ_{xy}(f) \tag{2}$$

where γ_{xy} is the coherence between two points x and y, S_{xy} is the cross-spectrum, and S_{xx} and S_{yy} are the auto spectra. C_{xy} and Q_{xy} are the real and imaginary part of the coherence.

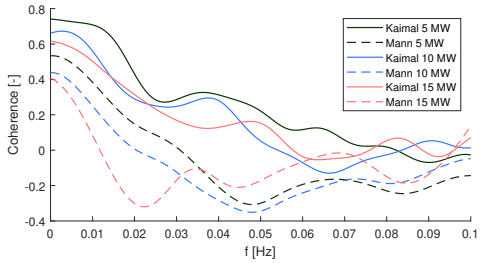

Figure 13. Spectral coherence between hub and outer rotor disk. Wind speed is 21 m/s.

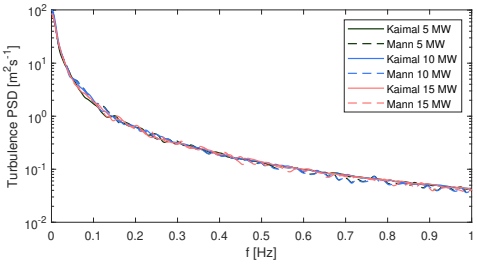

Figure 14. Hub-height wind turbulence spectrum at 15 m/s.

The coherence for wind speed 21 m/s is shown in Figure 13. Two effects are seen: The coherence decreases with increasing rotor disk area, and the coherence is higher for the Kaimal model than the Mann model. The effect of the former is that the 5-MW turbine will see more consistent variations in the wind speed across the rotor disk and higher variations in the effective wind speed. Similarly, the higher coherence with the Kaimal model will introduce higher variations in the effective wind speed than the Mann model. The expected consequence of this is higher variations in thrust force higher fatigue damage when the coherence is high.

The second property of interest the power spectral density (PSD) of the wind speed. As the Mann model has been adapted to give the same spectral properties as Kaimal, the spectra are expected to be similar. This is confirmed in Figure 14 for mean wind speed 15 m/s. The same is seen for the other wind speeds in the study.

5.2. Tower Top Response

The wind field is translated to structural response through the aerodynamic loads. While these loads are in turn influenced by the structural response, the loads from the rotor with a nacelle prevented from moving can provide a clearer picture of the difference between the wind models. This is particularly true for the tower top fore-aft bending moment, as shown in Figure 15. At low frequencies, the spectral value of the aerodynamic moment is higher when applying the Kaimal model. This corresponds well with the lower correlation of the Mann model. At higher frequencies the aerodynamic moment predicted by the Mann model is higher than the Kaimal moment, particularly visible at the 3P frequencies. This has been observed also by e.g. Bachynski & Eliassen[12] and Wise & Bachynski[13], and occurs despite the spectral density of the wind speed being equal. Note that the spectra in Figure 15 are normalized by the moment caused by the rated thrust force, M_{thrust}.

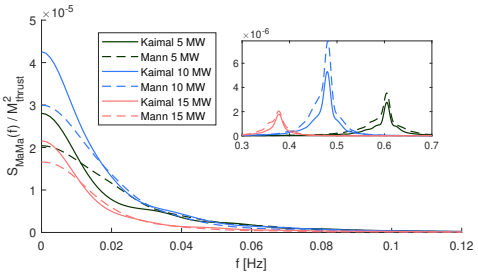

Figure 15. Aerodynamic moment at tower top for wind speed 15 m/s with a fixed rotor position.

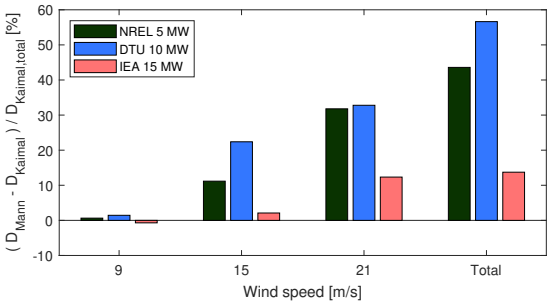

Figure 16. Differences in fatigue damage at tower top when using Kaimal and Mann turbulence models.

The total response and the effect on the fatigue damage is a combination of the higher response from the Kaimal model at low frequencies and the Mann model at higher frequencies. As the response at higher frequencies has more load cycles than the response at low frequencies, the influence on the fatigue damage will be higher than what is apparent from the PSDs.

Figure 16 shows how these effects add up at the tower top. The height of each bar is the difference between the fatigue damage predicted by the Kaimal and Mann models at each wind speed, normalized by the total fatigue damage predicted by the Kaimal model. The first observation is that the difference between the models increases with the wind speed. Secondly, the Mann model consistently predicts a higher fatigue damage, with the exception of the 15-MW turbine at wind speed 9 m/s. The difference between the fatigue damage predictions from the Kaimal and Mann models at the tower top are therefore dominated by the higher 3P response.

5.3. Tower Base Response

While the response at tower top can be understood from the aerodynamic loads, the structural dynamics become more important at the tower base. For the 5-MW turbine, the response is dominated by the low frequencies, as shown in Figure 17. At these frequencies the Kaimal model yields the highest response, including at the 1st natural frequency of the turbine.

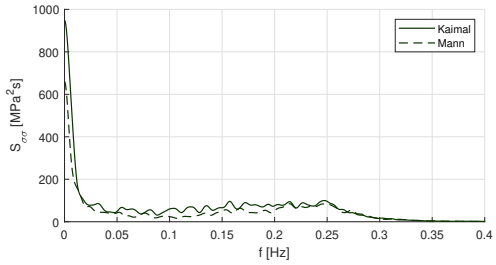

Figure 17. Upwind stress spectra at tower base for the 5-MW turbine in operational conditions, wind speed 15 m/s

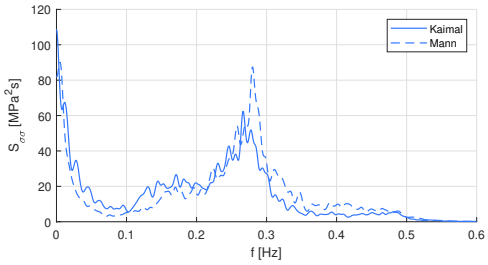

Figure 18. Upwind stress spectra at tower base for the 10-MW turbine in operational conditions, wind speed 15 m/s

The higher natural frequency of the 10-MW turbine reduces the difference between the two models at the natural frequency, as shown in Figure 18. As high-frequency (3P) loads become less important at low wind speeds, the Kaimal model predicts the highest fatigue damage at the two lowest wind speeds. The Mann model gives the highest fatigue damage at 21 m/s and in total, as shown in Figure 19.

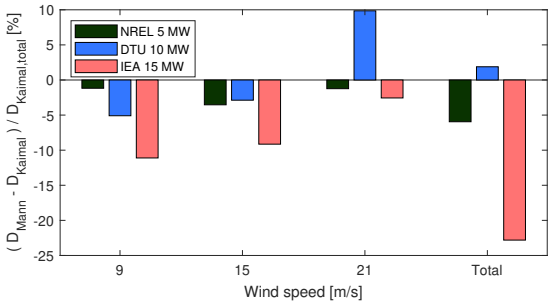

Figure 19. Differences in fatigue damage at tower base when using Kaimal and Mann turbulence models.

The 15-MW turbine has its natural frequency between the 5-MW and 10-MW turbines. This means that the Kaimal model predicts the highest fatigue damage for all wind speeds, but with the difference between the models decreasing as the wind speed increases.

5.4. Seafloor Response

The response at seafloor is primarily dominated by the wave loads. Still, the wind model influences the response also here. The differences in response are governed by the same mechanisms as at the tower base, but the majority of the response at seafloor is found at the wave frequencies. This means that the overall response is less influenced by the wind loads, giving less sensitivity to the choice of turbulence model.

5.5. Interaction with Uncertain Design Parameters

The interaction between the coherence model and the uncertain site parameters described in Section 2.6 was investigated. This was done in a similar manner to the soil model investigation in Section 4.4. However, no significant correlations were found between the wind coherence model and any single site parameter.

6. Discussion and Conclusion

The study has looked into the effect of modelling the soil-structure interaction by the use of p-y curves and a macro element, as well as the effect of modelling wind coherence using the Kaimal and Mann models. All model variations had effects that both increased and decreased the fatigue predictions compared to the alternative models. As an analyst it is important to be aware of how these models influence a specific turbine model to ensure conservative results.

For the soil model variations there, is a difference in both the predicted stiffness and damping. While the smallest turbine was most sensitive to the hysteretic effects, the largest uncertainty seems to be introduced by the calibration of the models. Although the macro element in general is expected to capture the response more accurately[6], the results from this paper highlight the importance of considering the calibration uncertainty. This may vary between the models, and a model with low calibration uncertainty should if possible be used in the analyses.

When considering the wind coherence models, the Kaimal model yields a higher response at low frequencies. The Mann model predicts a higher response at higher frequencies. This is particularly important for the 3P response. Additionally, the frequency where the change between which of the two coherence models that predicts the highest response is close to the 1st natural frequency of the foundations. A support structure with a low natural frequency tends to have highest response prediction from the Kaimal model, while a high natural frequency will give more conservative results using the Mann model.

Acknowledgments
This work has been carried out at the Centre for Autonomous Marine Operations and Systems (AMOS). The Norwegian Research Council is acknowledged as the main sponsor of NTNU AMOS. This work was supported by the Research Council of Norway through the Centres of Excellence funding scheme, project number 223254 - AMOS.

Appendix A

Table 2. Design parameters varied throughout the study and the associated data sources/references. For details, se Sørum et al.[21].

Parameter	Reference/Data source
Wind speed distribution	NORA10[20]
Wind direction	NORA10[20]
Turbulence intensity	FINO1[28]
Wind shear	FINO1[28]
Yaw error	Veldkamp[29]
Significant wave height	NORA10[20]
Wave peak period	NORA10[20]
Wind-wave misalignment	NORA10[20]
Marine growth thickness	Jusoh & Wolfram[30]
Monopile drag coefficient	Peering & Bedon[31], Veldkamp[29]
Soil undrained shear strength	Lacasse & Nadim[32]
Soil void ratio	Lacasse & Nadim[32]
Monopile diameter	Zaaijer[3], Hübler et al.[33]
SN curve parameters	DNV GL[27]
Fatigue capacity	Folsø et al.[34], Peering & Bedon[31]
Turbine availability	DNV GL[35], Pfaffel et al.[36], Larsen et al.[37]

References

[1] Wu X, Hu Y, Li Y, Yang J, Duan L, Wang T, Adcock T, Jiang Z, Gao Z, Lin Z, Borthwick A and Liao S 2019 Renewable and Sustainable Energy Reviews **104** 379–393
[2] Byrne B W, McAdam R, Burd H J, Houlsby G T, Martin C M, Zdravkovi L, Taborda D M G, Potts D M, Jardine R J, Sideri M, Schroeder F C, Gavin K, Doherty P, Igoe D, Muirwood A, Kallehave D and Skov Gretlund J New design methods for large diameter piles under lateral loading for offshore wind applications 3rd International Symposium on Frontiers in Offshore Geotechnics, ISFOG 2015, June 10, 2015 - June 12, 2015 Frontiers in Offshore Geotechnics III - Proceedings of the 3rd International Symposium on Frontiers in Offshore Geotechnics, ISFOG 2015 (CRC Press/Balkema) pp 705–710
[3] Zaaijer M B 2006 Applied Ocean Research **28** 45–57
[4] Page A M, Schafhirt S, Eiksund G R, Skau K S, Jostad H P and Sturm H June 26-July 1, 2016 Alternative numerical pile foundation models for integrated analyses of monopile-based offshore wind turbines Proceedings of the Twenty-sixth (2016) International Ocean and Polar Engineering Conference (Rhodos, Greece: International Society of Offshore and Polar Engineers) pp 111–119
[5] Aasen S, Page A M, Skjolden Skau K and Nygaard T A 2017 Wind Energ. Sci. **2** 361–376
[6] Page A M, Grimstad G, Eiksund G R and Jostad H P 2018 Ocean Engineering **167** 23–35
[7] Page A, Grimstad G, Eiksund G and Jostad H P 2019 Computers and Geotechnics **Vol. 106** 314–326
[8] Katsikogiannis G, Bachynski E E and Page A M 2019 Journal of Physics: Conference Series **1356** 012019
[9] IEC 2019 International Electrotechnical Commission, Design Requirements for fixed offshore wind turbines (IEC 61400-3)
[10] Myrtvedt M H, Nybø A and Nielsen F G 2020 Journal of Physics: Conference Series **1669** 012013

[11] Nybø A, Nielsen F G and Godvik M 2021 Wind Energy **24** 1482–1500
[12] Bachynski E E and Eliassen L 2019 Wind Energy **22** 219–238
[13] Wise A S and Bachynski E E 2020 Wind Energy **23** 1266–1285
[14] Jonkman J, Butterfield S, Musial W and Scott G 2009 Definition of a 5MW reference wind turbine for offshore system development Report National Renewable Energy Laboratory (NREL) Denver, CO, US
[15] Bak C, Zahle F, Bitsche R, Kim T, Yde A, Henriksen L C, Andersen P B, Natarajan A and Hansen M To be accepted J. Wind Energy
[16] Gaertner E, Rinker J, Sethuraman L, Zahle F, Anderson B, Barter G, Abbas N, Meng F, Bortolotti P, Skrzypinski W, Scott G, Feil R, Bredmose H, Dykes K, Sheilds M, Allen C and Viselli A 2020 Definition of the IEA 15-megawatt offshore reference wind turbine Tech. rep. International Energy Agency Denver, CO, US URL `https://www.nrel.gov/docs/fy20osti/75698.pdf`
[17] Jonkman J and Musial W 2010 Offshore code comparison collaboration (OC3) for IEA task 23 offshore wind technology and deployment Report NREL Golden, Colorado, USA
[18] Velarde J and Bachynski E E 2017 Energy Procedia **137** 3–13
[19] Katsikogiannis G, Sørum S H, Bachynski E E and Amdahl J 2021 Marine Structures **77** 102939
[20] Reistad M, Breivik O, Haakenstad H, Aarnes O J, Furevik B R and Bidlot J R 2011 Journal of Geophysical Research: Oceans **116** 1–18
[21] Sørum S H, Katsikogiannis G, Bachynski-Polić E E, Amdahl J, Page A M and Klinkvort R T Accepted to Wind Energy
[22] MacCamy RC, Fuchs R A 1954 Wave Forces on Piles: A Diffraction Theory Tech. rep. Office of Naval Research, U. S. Department of the Navy Washington, D.C., US
[23] SINTEF Ocean 2017 SIMO 4.10.3 user guide Tech. rep. SINTEF Ocean Trondheim, Norway
[24] SINTEF Ocean 2017 RIFLEX 4.10.3 user guide Tech. rep. SINTEF Ocean Trondheim, Norway
[25] Klinkvort R T, Sturm H, Page A M, Zhang Y and Jostad H P August 28–31, 2022 A consistent, rigorous and super-fast monopile design approach Proceedings of the 4th International Symposium on Frontiers in Offshore Geotechnics (Austin, Texas, US: American Society of Civil Engineers)
[26] WAFO-group 2011 WAFO - A Matlab Toolbox for Analysis of Random Waves and Loads - A Tutorial
[27] DNV-GL (Det Norske Veritas - Germanischer Lloyd) Fatigue design of offshore steel structures (DNVGL-RP-C203)
[28] Bundesamt für Seeschifffahrt und Hydrographie FINO - datenbankinformationen
[29] Veldkamp H F 2006 Chances in wind energy: a probalistic approach to wind turbine fatigue design Thesis Delft University Delft, NL
[30] Jusoh I and Wolfram J 1996 Jurnal Mekanikal **1**
[31] Peeringa J and Bedon G 2017 Energy Procedia **137** 255–260
[32] Lacasse S and Nadim F 1996 Uncertainties in characterising soil properties Uncertainty in the geologic environment: from theory to practice (Madison, Wisconsin: American Society of Civil Engineers)
[33] Hübler C, Gebhardt C G and Rolfes R 2017 Renewable Energy **111** 878–891
[34] Folsø R, Otto S and Parmentier G 2002 Marine Structures **15** 627–651
[35] DNV-GL (Det Norske Veritas - Germanischer Lloyd) 2016 Loads and site conditions for wind turbines (DNVGL-ST-0437)
[36] Pfaffel S, Faulstich S and Rohrig K 2017 energies **10** 1904
[37] Larsen J, Soerensen H, Christiansen E and Naef S October 26-28, 2005 Experiences from Middelgrunden 40 MW offshore wind farm Copenhagen Offshore Wind (Copenhagen: Danish Wind Industry Association)